

# BRAIN COMMUNICATIONS

## Objective interictal electrophysiology biomarkers optimize prediction of epilepsy surgery outcome

Naoto Kuroda,<sup>1,2,\*</sup>  Masaki Sonoda,<sup>1,3,\*</sup> Makoto Miyakoshi,<sup>4</sup> Hiroki Nariai,<sup>5</sup> Jeong-Won Jeong,<sup>1,6</sup> Hirotaka Motoi,<sup>1,7</sup> Aimee F. Luat,<sup>1,6</sup> Sandeep Sood<sup>8</sup> and Eishi Asano<sup>1,6</sup>

\* These authors contributed equally to this work.

Researchers have looked for rapidly- and objectively-measurable electrophysiology biomarkers that accurately localize the epileptogenic zone. Promising candidates include interictal high-frequency oscillation and phase-amplitude coupling. Investigators have independently created the toolboxes that compute the high-frequency oscillation rate and the severity of phase-amplitude coupling. This study of 135 patients determined what toolboxes and analytic approaches would optimally classify patients achieving post-operative seizure control. Four different detector toolboxes computed the rate of high-frequency oscillation at  $\geq 80$  Hz at intracranial EEG channels. Another toolbox calculated the modulation index reflecting the strength of phase-amplitude coupling between high-frequency oscillation and slow-wave at 3–4 Hz. We defined the completeness of resection of interictally-abnormal regions as the subtraction of high-frequency oscillation rate (or modulation index) averaged across all preserved sites from that averaged across all resected sites. We computed the outcome classification accuracy of the logistic regression-based standard model considering clinical, ictal intracranial EEG and neuroimaging variables alone. We then determined how well the incorporation of high-frequency oscillation/modulation index would improve the standard model mentioned above. To assess the anatomical variability across non-epileptic sites, we generated the normative atlas of detector-specific high-frequency oscillation and modulation index. Each atlas allowed us to compute the statistical deviation of high-frequency oscillation/modulation index from the non-epileptic mean. We determined whether the model accuracy would be improved by incorporating absolute or normalized high-frequency oscillation/modulation index as a biomarker assessing interictally-abnormal regions. We finally determined whether the model accuracy would be improved by selectively incorporating high-frequency oscillation verified to have high-frequency oscillatory components unattributable to a high-pass filtering effect. Ninety-five patients achieved successful seizure control, defined as International League against Epilepsy class 1 outcome. Multivariate logistic regression analysis demonstrated that complete resection of interictally-abnormal regions additively increased the chance of success. The model accuracy was further improved by incorporating z-score normalized high-frequency oscillation/modulation index or selective incorporation of verified high-frequency oscillation. The standard model had a classification accuracy of 0.75. Incorporation of normalized high-frequency oscillation/modulation index or verified high-frequency oscillation improved the classification accuracy up to 0.82. These outcome prediction models survived the cross-validation process and demonstrated an agreement between the model-based likelihood of success and the observed success on an individual basis. Interictal high-frequency oscillation and modulation index had a comparably additive utility in epilepsy pre-surgical evaluation. Our empirical data support the theoretical notion that the prediction of post-operative seizure outcomes can be optimized with the consideration of both interictal and ictal abnormalities.

- 1 Department of Paediatrics, Children's Hospital of Michigan, Detroit Medical Centre, Wayne State University, Detroit, MI 48201, USA
- 2 Department of Epileptology, Tohoku University Graduate School of Medicine, Sendai 9808575, Japan
- 3 Department of Neurosurgery, Yokohama City University, Yokohama 2360004, Japan

Received October 15, 2020. Revised January 9, 2021. Accepted February 2, 2021. Advance Access publication March 14, 2021

© The Author(s) (2021). Published by Oxford University Press on behalf of the Guarantors of Brain.

This is an Open Access article distributed under the terms of the Creative Commons Attribution License (<http://creativecommons.org/licenses/by/4.0/>), which permits unrestricted reuse, distribution, and reproduction in any medium, provided the original work is properly cited.

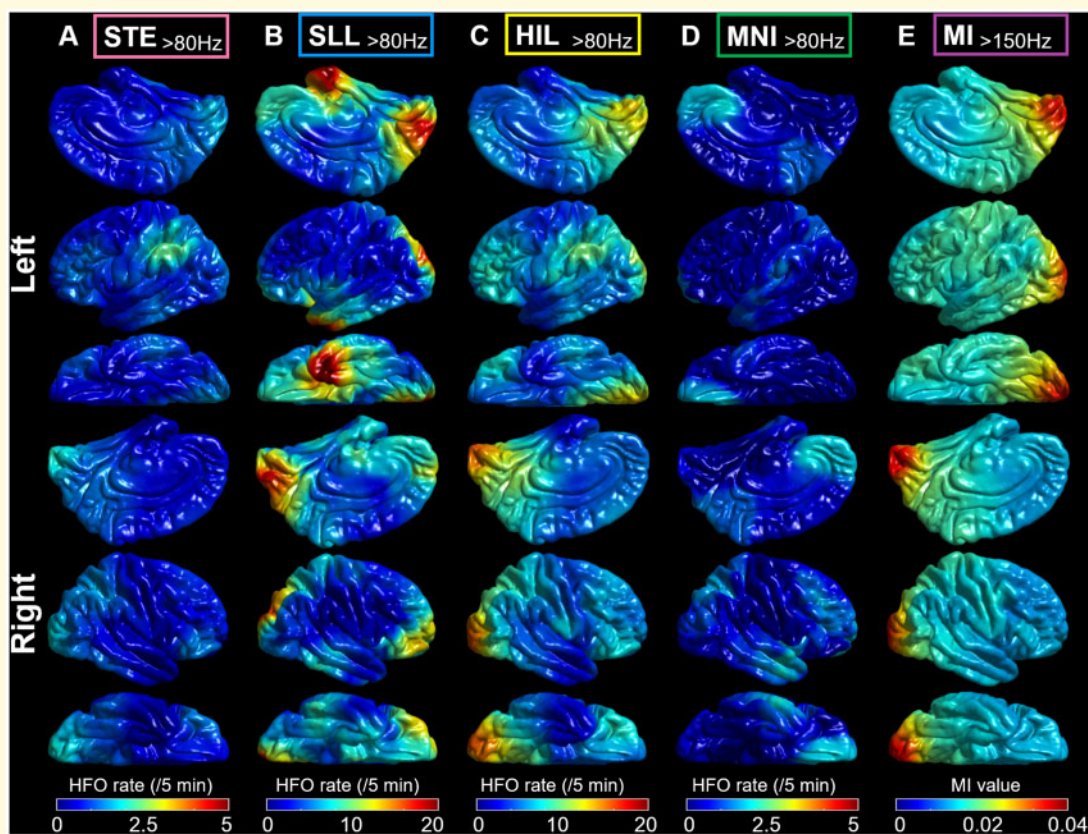
- 4 Swartz Centre for Computational Neuroscience, Institute for Neural Computation, University of California San Diego, La Jolla, CA 92093, USA
- 5 Division of Paediatric Neurology, Department of Paediatrics, UCLA Mattel Children's Hospital, David Geffen School of Medicine, Los Angeles, CA 90095, USA
- 6 Department of Neurology, Children's Hospital of Michigan, Detroit Medical Centre, Wayne State University, Detroit, MI 48201, USA
- 7 Department of Paediatrics, Yokohama City University Medical Centre, Yokohama 2320024, Japan
- 8 Department of Neurosurgery, Children's Hospital of Michigan, Detroit Medical Centre, Wayne State University, Detroit, MI 48201, USA

Correspondence to: Eishi Asano, MD, PhD, MS (CRDSA)  
 Division of Paediatric Neurology,  
 Children's Hospital of Michigan, Wayne State University  
 3901 Beaubien Street, Detroit, MI 48201, USA  
 E-mail: easano@med.wayne.edu

**Keywords:** invasive recording; electrocorticography (ECoG); high-frequency oscillation (HFO); modulation index (MI); phase-amplitude coupling (PAC)

**Abbreviations:** AEDs = antiepileptic drugs; AUC = area under the curve; HFO = high-frequency oscillation; HIL = Hilbert; iEEG = intracranial EEG; ILAE = International League against epilepsy; MI = modulation index; MNI = Montreal Neurological Institute; RMS = root mean square; ROC = receiver-operating characteristics; SDs = standard deviations; SLL = short line length; SOZ = seizure-onset zone; STE = short time energy

### Graphical Abstract



## Introduction

Complete resection of the epileptogenic zone is necessary to achieve successful seizure control in drug-resistant focal epilepsy.<sup>1</sup> Clinicians at tertiary epilepsy centres across the world frequently rely on the seizure-onset zone

(SOZ) defined on intracranial EEG (iEEG) and an MRI lesion to localize the epileptogenic zone.<sup>2,3</sup> To optimize the diagnostic accuracy, investigators look for rapidly- and objectively-measurable electrophysiology biomarkers. We previously hypothesized that the rate of interictal spike discharges on iEEG would provide additive

information to localize the epileptogenic zone and effectively improve the prediction of post-operative seizure outcomes. Previous iEEG studies indeed demonstrated that the SOZ was associated with increased spiking rates.<sup>4,5</sup> However, our prospective iEEG study failed to prove that considering spike rates improves the seizure outcome classification model-based on the standard information, including clinical, SOZ and MRI data.<sup>6</sup> Thus, we have looked for an alternative electrophysiology biomarker.

The promising biomarkers include interictal high-frequency oscillation (HFO), episodic and spontaneous iEEG signals at  $\geq 80$  Hz, augmenting in amplitude and standing out from the baseline.<sup>7,8</sup> Investigators provide the open-source detectors, which automatically detect HFO events according to the own definition of HFO.<sup>9–13</sup> The SOZ was reported to show higher HFO rates than the non-SOZ, whereas the effect size differed between studies.<sup>13–16</sup> Investigators, who assessed the seizure outcome in relation to the extent of resection, further supported the utility of interictal HFO in epilepsy presurgical evaluation.<sup>17</sup> A prospective iEEG study of 52 patients found a correlation between the removal of HFO-generating regions and seizure outcomes at the group level.<sup>18</sup> In the present study, four open-source detectors computed the HFO rate at iEEG electrode sites.<sup>9–12</sup> We investigated whether the incorporation of HFO rates would improve the standard outcome classification model considering the clinical, SOZ and MRI data achievable by the completion of resective surgery. We determined whether HFO rates quantified by different detectors would commonly enhance the accuracy of the outcome classification model.

The present study likewise assessed the diagnostic utility of phase-amplitude coupling between interictal HFO and slow-wave, rated by modulation index (MI).<sup>19,20</sup> Since the present study has chosen to quantify the magnitude of high-frequency amplitude  $\geq 80$  Hz stereotypically coupled with subsequent slow-wave 3–4 Hz, MI effectively reflects the severity of spike-and-wave discharges.<sup>21,22</sup> Two epilepsy centres independently reported that the phase-amplitude coupling was elevated at the SOZ; thereby, the coupling with slow-wave at 3–4 Hz best differentiated the SOZ from non-SOZ.<sup>23,24</sup> We determined whether the standard outcome classification model would be improved by incorporating MI more than consideration of HFO, or *vice versa*.

The present study followed the recommendation to consider the anatomical variability in the HFO rate across non-epileptic sites in surgical planning.<sup>25,26</sup> We generated the normative atlas of detector-specific HFO and MI; thus, each atlas allowed us to compute the statistical deviation (z-score) of HFO/MI from the normative mean using the concept of statistical parametric mapping.<sup>27</sup> We determined whether the post-operative seizure outcome would be classified better by incorporating absolute or z-score normalized HFO/MI (referred to as zHFO/zMI below).

The present study finally determined whether investigators must selectively use HFO events verified to have

distinct high-frequency oscillatory components unattributable to the results from a high-pass filtering effect on a very sharply-contoured transient.<sup>28–30</sup> It remains to be determined whether such verified HFO (vHFO) would allow investigators to predict post-operative seizure outcomes more accurately. We determined whether the post-operative seizure outcome would be classified better by incorporating vHFO as defined by each of the four different detectors.

## Materials and methods

### Patients

We studied a consecutive series of 135 patients with drug-resistant focal epilepsy (Table 1) who underwent resective surgery between January 2007 and May 2018 at Detroit Medical Centre in Detroit, USA. The inclusion criteria included extraoperative iEEG recording with a sampling rate of 1000 Hz.<sup>11,31</sup> The exclusion criteria included (i) diagnosis of bilateral multifocal epilepsy purely based on the Phase-1 non-invasive presurgical evaluation,<sup>32</sup> (ii) callosotomy, hemispherotomy, or hemispherectomy,<sup>33,34</sup> (iii) major brain malformations making the central or lateral sulcus unidentifiable,<sup>35</sup> (iv) malignant brain tumour suspected on preoperative MRI,<sup>31</sup> (v) post-operative follow-up shorter than 1 year,<sup>36</sup> (vi) age at surgery was  $< 4$  years<sup>37</sup> and (vii) history of previous resective epilepsy surgery.<sup>27</sup> The institutional review board at Wayne State University has approved the protocol. We obtained written informed consent from patients or the guardians of paediatric patients.

### iEEG

We placed platinum subdural electrodes for the SOZ localization.<sup>6,31,35</sup> Subdural electrodes remain utilized in many paediatric epilepsy centres across the countries.<sup>38–42</sup> Surface electrooculography and electromyography electrodes determined the onset of seizure-related symptoms and sleep staging.<sup>31,43</sup> We recorded video-iEEG signals for 2–7 days with an amplifier band-pass of 0.016–300 Hz and performed analysis using common average reference.<sup>43,44</sup> We discontinued antiepileptic drugs (AEDs) and resumed them following the localization of the SOZ.<sup>6</sup> We excluded artifactual channels from further analyses.<sup>44</sup> Thus, a total of 14 604 electrode channels were available for analysis.

### MRI

Preoperative 3 T MRI data, including T1-weighted three-dimensional spoiled gradient-echo volumetric scan and fluid-attenuated inversion recovery scan, were reviewed by an experienced neuroradiologist.<sup>31,32</sup> Implanted subdural electrodes were co-registered with a three-dimensional surface image.<sup>35,45</sup> Using the FreeSurfer scripts

**Table 1 Patient profile**

Patients profile	
<b>Total number of patients</b>	<b>135</b>
Mean age	13.1 years old (range: 4–44)
Sex	68 males (50.4%)
Daily seizures	45 patients (33.3%)
Number of AEDs	
One AED	40 patients (29.6%)
Two AEDs	60 patients (44.4%)
Three AEDs	34 patients (25.2%)
Four AEDs	None (0%)
Five AEDs	1 patient (0.7%)
Left-hemispheric epilepsy	71 patients (52.6%)
Lesion visible on MRI	79 patients (58.5%)
Habitual seizures captured during iEEG recording	117 patients (86.7%)
Incomplete resection of SOZ	17 patients (12.6%)
Necessity to resect extra-temporal region	85 patients (63.0%)
Mean size of resection (%)	16.2% (range: 0.6–91.6)
Mean number of analysed electrodes per patient	108.2 electrodes (range: 32–152)
ILAE class I outcome	95 patients (70.4%)

AEDs = antiepileptic drugs taken immediately before the electrode placement; iEEG = intracranial EEG; SOZ = seizure-onset zone; ILAE = International League Against Epilepsy.

(<http://surfer.nmr.mgh.harvard.edu>. Accessed 22 March 2021), we created the averaged surface image to which all electrode locations were spatially normalized.<sup>27,35,37</sup> The averaged surface image functioned as the template for the normative HFO/MI atlas.

## Surgery

Our previous studies described the principle to determine the extent of cortical resection.<sup>6,31</sup> We intended to remove the SOZ and a neighbouring MRI lesion, if any, while maximally preserving the eloquent cortex. None of the clinicians or investigators were aware of quantitative HFO/MI analysis results before the resective surgery.

Using the intraoperative photographs immediately before dural closure, we prospectively declared whether the SOZ was removed entirely.<sup>31</sup> The FreeSurfer scripts computed the extent of resection (i.e. percentage of the hemisphere).<sup>31</sup> Post-operative MRI cannot function as a pre-operative predictor. Using the Spearman's rank test, our ancillary analysis assessed the concordance between the resection sizes estimated by intraoperative photographs and post-operative MRI in 89 patients whose post-operative MRI data were available to us (Supplementary Fig. 1).

## Computation of the rate of HFO

We used MATLAB R2019a (Mathworks, Natick, MA) for the following HFO analyses. The visual assessment initially identified the earliest, artifact-free, 5-min slow-wave sleep >2h apart from ictal events<sup>31</sup>; then, the RIPPLELAB (<https://github.com/BSP-Uniandes/RIPPLELAB/>. Accessed 22 March 2021)<sup>13</sup> quantified the rate of HFO events at each electrode site. The RIPPLELAB incorporates four distinct HFO detection algorithms as follows: (i) Short Time Energy (STE) method,<sup>9</sup> (ii) Short Line Length (SLL)

method,<sup>10</sup> (iii) Hilbert (HIL) method<sup>11</sup> and (iv) Montreal Neurological Institute (MNI) method.<sup>12</sup> We used the default settings as incorporated in the RIPPLELAB<sup>13</sup> (Supplementary Fig. 2A–D) and each HFO detection algorithm computed the rates of HFO $\geq$ 80 Hz, HFO $\geq$ 150 Hz and HFO $\geq$ 250 Hz. Each original article describes a given detector's principle in detail.<sup>9–12</sup> In short, the STE method-defined an HFO event as an iEEG segment showing successive root mean square values greater than 5 SDs above the overall root mean square mean, including more than 6 peaks >3 SDs on the band-pass filtered iEEG.<sup>9</sup> The SLL method-defined an HFO as a segment showing SLL-based amplitude augmentation greater than the 97.5th percentile of the empirical cumulative distribution function computed on band-pass filtered iEEG signals.<sup>10,13</sup> The HIL method-defined an HFO as a segment showing HIL transform-based envelope augmentation greater than five SDs.<sup>11</sup> The MNI method-defined an HFO as a segment showing root mean square-based energy above the 99.9999th percentile compared to the baseline if such a baseline period was considered to be present.<sup>12</sup> If the baseline was absent, the MNI method treated a segment showing the  $\geq$ 95th percentile of the cumulative distribution function as computed from the 1 min band-passed iEEG.

Below, for example, STE $_{>f}$  Hz denotes the STE method-defined HFO in the frequency range at  $f$ -300 Hz; thereby,  $f$  was 80, 150, or 250.

## Computation of MI

All iEEG data points during the 5 min mentioned above were HIL transformed by the EEGLAB Toolbox winPACT (<https://sccn.ucsd.edu/wiki/WinPACT>. Accessed 22 March 2021).<sup>20</sup> The toolbox automatically computed the MI quantifying the strength of coupling between

HFO amplitude and the instantaneous phase of slow-wave<sub>3-4Hz</sub> (Supplementary Fig. 2E).<sup>27,31</sup> Below,  $MI_{>f}$  Hz denotes the coupling between the amplitude of  $HFO_{f-300Hz}$  and the phase of slow-wave<sub>3-4Hz</sub>; thereby,  $f$  was 80, 150, or 250.

## Post-operative seizure outcome

Post-operative seizure outcome was classified at the last follow-up according to the International League Against Epilepsy (ILAE) classification.<sup>36</sup> The Class-1 was treated as a success.<sup>27,31</sup>

## Normative atlas

We generated the normative atlases of HFO defined by four detectors mentioned above. We used the method used to create the normative MI atlas based on the 2477 non-epileptic electrode sites sampled from 47 patients.<sup>27</sup> Non-epileptic sites were defined as those outside the SOZ, cortical lesions and spiking zones.<sup>25</sup> We computed the mean and standard deviation of the HFO rate at each surface model mesh vertex based on the 60 closest

non-epileptic sites. Figure 1 visualizes the mean non-epileptic HFO rate and MI at the whole-brain level.

## Statistical analysis

We used SPSS v25 (IBM, Armonk, NY) and considered a two-sided  $P$ -value of 0.05 as significant. We determined how accurately the standard model incorporating the following 10 variables would classify patients achieving a surgical success (i.e. ILAE class 1 outcome). The predictor variables included (i) age, (ii) sex, (iii) presence of daily seizures, (iv) number of oral AEDs taken immediately before the intracranial electrode placement (reflecting the severity of seizure burden),<sup>46</sup> (v) affected hemisphere, (vi) presence of an MRI lesion,<sup>47</sup> (vii) whether iEEG recording captured habitual seizure events, (viii) whether the SOZ was completely removed, (ix) the necessity of extra-temporal lobe resection and (x) size of resection. We computed the  $R^2$  to assess the fitness of the standard model in outcome classification. The receiver-operating characteristics (ROC) analysis determined the model accuracy, as rated by the area under the ROC curve (AUC).

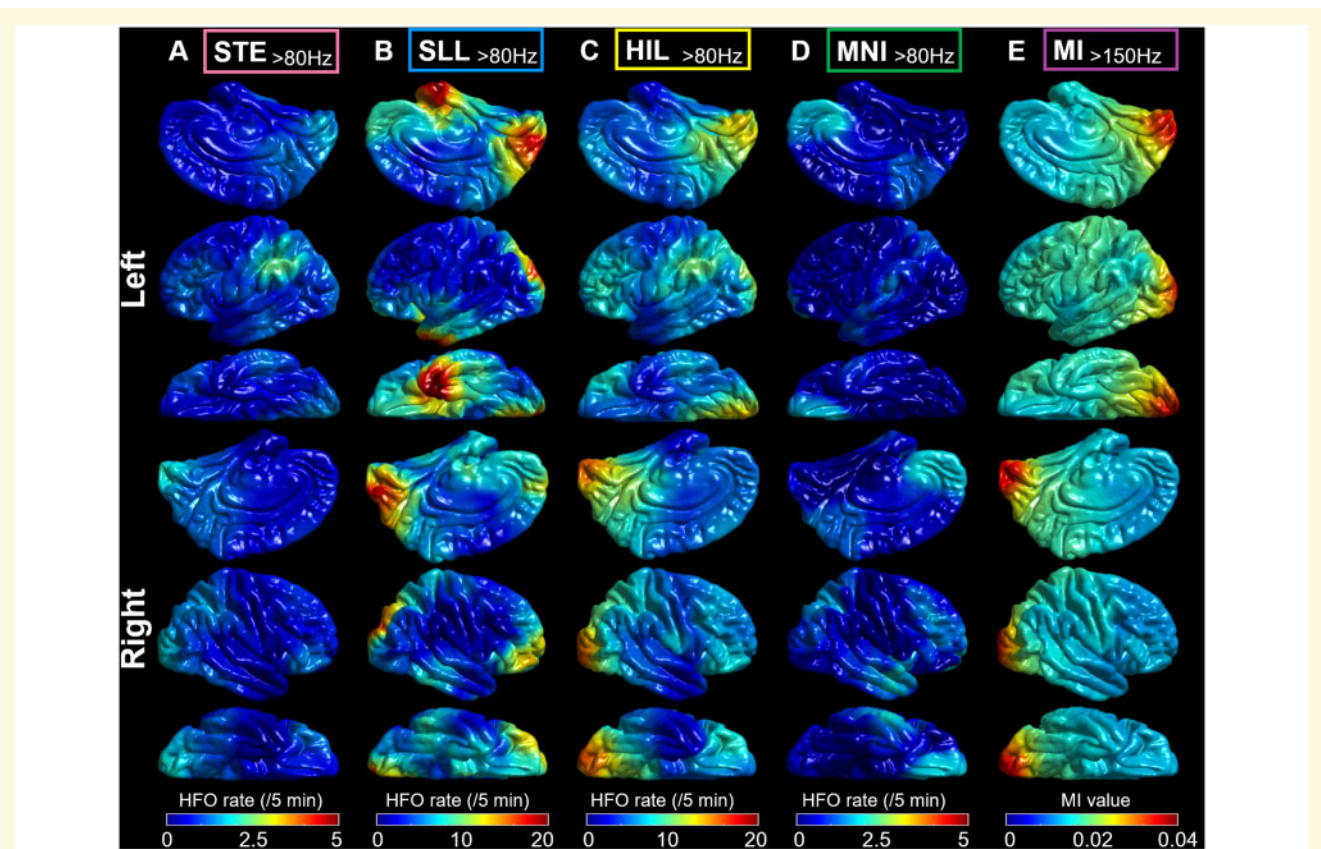


**Figure 1 Normative atlas of HFO and MI.** (A–D) Each normative atlas demonstrates the spatial characteristics of the rate of  $HFO_{>80Hz}$  defined by each of the four different detectors. The mean HFO rate across 60 closest non-epileptic sites is presented. Note that each atlas has excluded outlier non-epileptic sites showing HFO rates greater than ten standard deviations higher than the mean. (A) STE detector.<sup>9</sup> (B) SLL detector.<sup>10</sup> (C) HIL detector.<sup>11</sup> (D) MNI detector.<sup>12</sup> (E) The normative atlas of  $MI_{>150Hz}$  shows the characteristics of phase-amplitude coupling between  $HFO_{>150Hz}$  and slow wave<sub>3-4Hz</sub>.

We determined how well incorporating the detector-specific HFO measures would improve the standard model's accuracy in seizure outcome classification. We computed the accuracy of a given HFO model as follows. Each detector-specific HFO model incorporated Subtraction-HFO in addition to the ten variables mentioned above. Subtraction-HFO was defined as the subtraction of the HFO rate averaged across all preserved sites from that averaged across all resected sites. Subtraction-HFO effectively quantified the completeness of the resection of interictal HFO-generating regions. Higher Subtraction-HFO inferred more complete resection of the area showing a focal increase of HFO rate.

With the ROC analysis, we likewise assessed how accurately the MI model, incorporating Subtraction-MI in addition to the 10 variables mentioned above, would classify patients who achieved surgical success. Subtraction-MI was defined as the subtraction of the MI averaged across all preserved sites from that averaged across all resected sites.

The subsequent analysis assessed the generalizability of the notion that investigators should consider the anatomical variability of HFO/MI across non-epileptic sites.<sup>25–27</sup> Specifically, each electrode site was assigned a z-score normalized HFO rate (zHFO) and MI (zMI), as computed using the normative mean and standard deviation across 60 closest non-epileptic channels (Fig. 1).<sup>27</sup> The ROC analyses likewise determined the outcome

classification accuracy of a given zHFO model and zMI model (i.e. that incorporating Subtraction-zHFO/zMI instead of Subtraction-HFO/MI). For interested readers, further analysis determined how many closest non-epileptic sites (range: 10–100) should be included for computing a z-score normalized HFO/MI that would result in an optimal classification of patients achieving surgical success (Fig. 2).

The subsequent analysis determined whether investigators must selectively use HFO events verified to have distinct high-frequency oscillatory components unattributable to the results from a high-pass filtering effect on a very sharply-contoured transient.<sup>28–30</sup> Such distinct high-frequency oscillatory components are reflected by a blob-like power increase on the time-frequency plot (Fig. 3B–D).<sup>28</sup> The auto-classify function, implemented in the RIPPLELAB<sup>13</sup>, verified whether each detected HFO event was unattributable to the filtering (Fig. 3). Based on the spectral characteristics, this function labelled each detected event as 'vHFO<sub>80–150Hz</sub>', 'vHFO<sub>150–250Hz</sub>', 'vHFO<sub>250–300Hz</sub>', 'Spike', 'Artifact', or 'Others'. Thereby, vHFO<sub>*f* Hz</sub> denotes HFO verified to have a distinct high-frequency oscillatory component at *f* Hz. This verification procedure was extremely time-consuming (up to three investigator hours/patient). We computed the rates of vHFO events; thereby, vHFO<sub>>80Hz</sub> included vHFO<sub>80–150Hz</sub>, vHFO<sub>150–250Hz</sub> and vHFO<sub>250–300Hz</sub>. Likewise, vHFO<sub>>150Hz</sub> included vHFO<sub>150–250Hz</sub> and

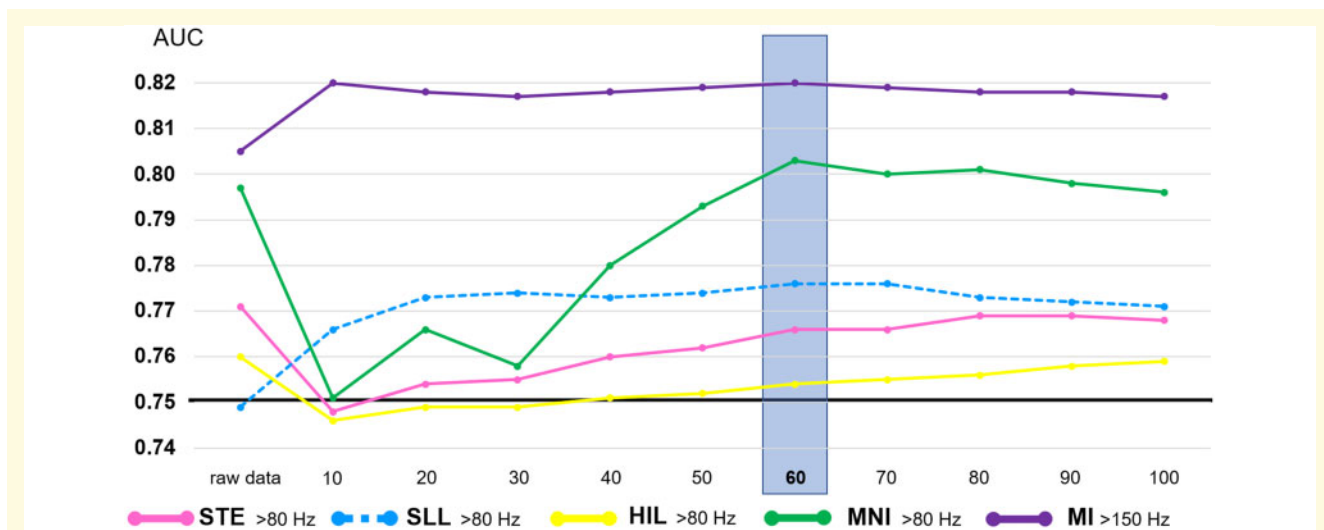


**Figure 2 Effect of the number of non-epileptic electrode sites included for computation of the normative mean/standard deviation.** We delineated how the classification accuracy of the zHFO and zMI models would be altered by the analytic approach (i.e. the number of non-epileptic sites to be included for computation of the normative mean and standard deviation). The classification accuracy of zHFO and zMI models was stable when  $\geq 60$  closest non-epileptic sites were included. Conversely, inclusion of as small as 10 non-epileptic sites resulted in a worsening of the classification accuracy by some zHFO models. This observation can be explained by the notion that these HFO detectors were designed to effectively avoid detecting HFO<sub>>80Hz</sub> at most non-epileptic sites and that the computation of standard deviation of HFO rate was not tenable with 10 closest sites. The one-way ANOVA test indicated that the accuracy of outcome classification differed among these five models ( $P < 0.001$ ). The post-hoc paired *t*-test indicated that the zMI model had higher classification accuracy compared to all zHFO models (Bonferroni-corrected  $P < 0.05$  on paired *t*-test). The standard model had a classification accuracy of 0.75 as indicated by a thick line. AUC: Area under the curve on the ROCs analysis.

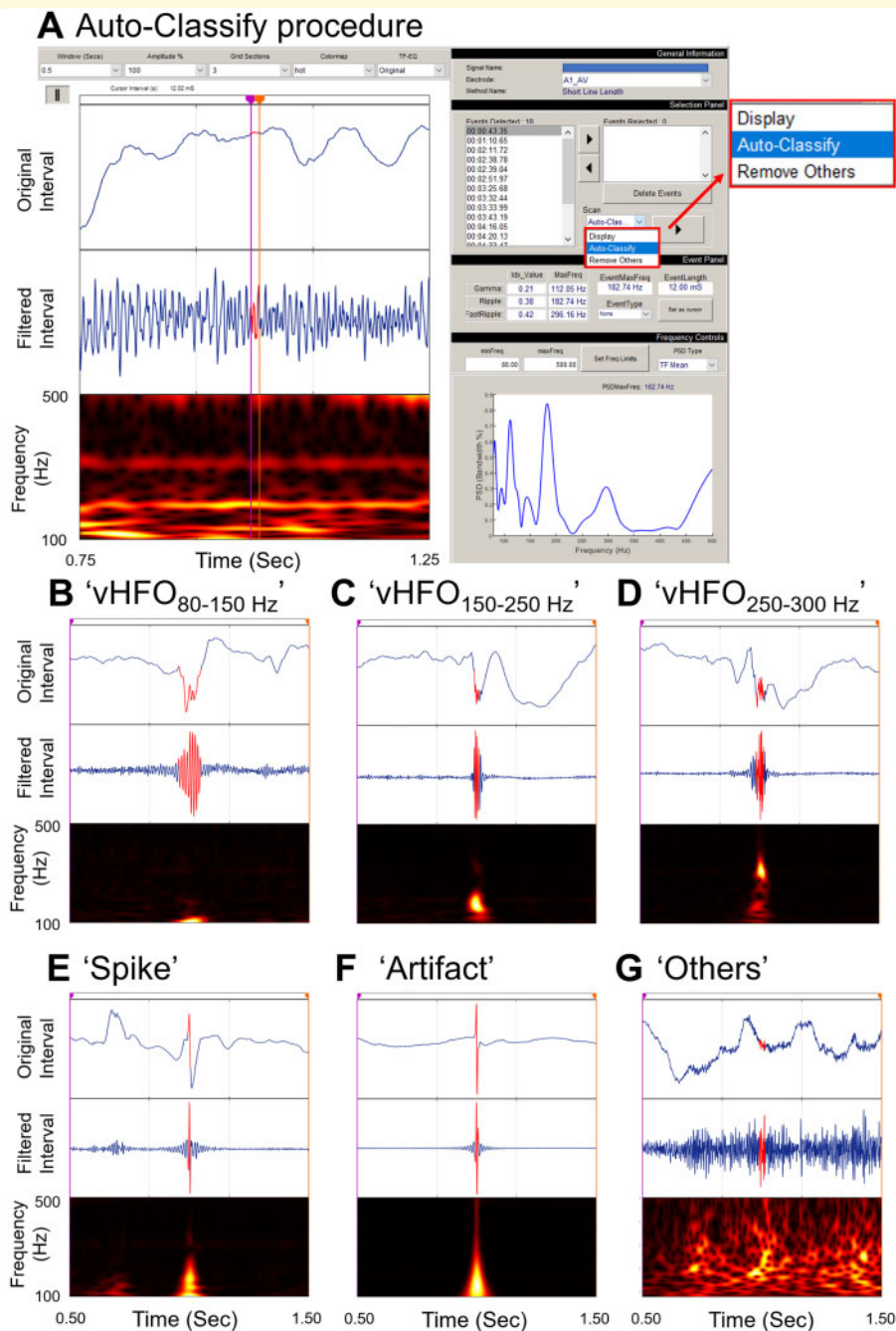


**Figure 3** Verification process using the RIPPLELAB. (A) The snapshot of HFO verification process using the auto-classify function implemented in the RIPPLELAB. Based on the spectral characteristics, this function allowed us to label each detected event of HFO as either B 'vHFO<sub>80-150 Hz</sub>', 'vHFO<sub>150-250 Hz</sub>' in C, 'vHFO<sub>250-300 Hz</sub>' in D, 'Spike' in E, 'Artifact' in F or 'Others' in G. vHFO<sub>80-150 Hz</sub> denotes an HFO event verified to have distinct high-frequency oscillatory components at 80–150 Hz unattributable to the results from an 80-Hz high-pass filtering on a very sharply-contoured transient. (B–G) Top image: Unfiltered intracranial EEG (iEEG) trace. Middle image: Filtered iEEG trace. Bottom image: Time-frequency plot.

vHFO<sub>250-300 Hz</sub>. We determined the outcome classification accuracy of a given vHFO model (i.e. that incorporating Subtraction-vHFO instead of Subtraction-HFO).

Leave-one-out analysis<sup>27</sup> cross-validated the standard outcome prediction model and each of those incorporating interictal electrophysiology biomarkers mentioned

above. We estimated the probability of surgical success of each new patient based on the multivariate logistic regression model incorporating all variables derived from the remaining 134 patients. The AUC of ROC curves determined how much the leave-one-out cross-validation altered each model's performance.

We finally measured the computational time (seconds/channel) required to quantify the HFO rate and MI. We used a Windows 10 laptop computer with Intel Core i7 at 2.7–2.9 GHz processor, 16.0 GB random-access memory and a 64-bit operating system (NEC Corporation, Tokyo, Japan).

## Data and code availability

All data and code used in this study are available upon request to the corresponding author. We are pleased to re-analyse the data and provide the results based on readers' specific suggestions to improve our understanding of the neurobiology of epilepsy.

## Results

### Post-operative seizure outcome

ILAE class 1, 2, 3, 4, 5 and 6 outcomes were noted in 95, 2, 15, 14, 9 and 0 patients (mean follow-up: 65.4 months [SD: 38.2; range: 12–130]).

## Resection size

The resection size estimated by the intraoperative photo was concordant with that by the post-operative MRI (Spearman rho: 0.95;  $P < 0.001$ ; Supplementary Fig. 1).

## Utility of the standard model in outcome classification

The standard model classified the post-operative seizure outcome with significance ( $R^2$ : 0.23,  $P = 0.008$ ). Incomplete SOZ resection (odds ratio [OR]: 0.15 [95%CI: 0.05–0.51]) and a larger number of AEDs (OR: 0.56 [0.33–0.97]) were independently associated with a smaller chance of success (Supplementary Table 1). The accuracy of outcome classification was 0.75, as rated by the AUC of the ROC curve (Fig. 4A).

## Normative atlas

Figure 1 presents the spatial distributions of detector-specific  $\text{HFO}_{>80\text{Hz}}$  and  $\text{MI}_{>150\text{Hz}}$  within non-epileptic sites. Non-epileptic occipital lobe sites were associated with higher  $\text{HFO}_{>80\text{Hz}}$  rates compared to other lobes ( $P < 0.001$  on the linear mixed model analysis). The SLL

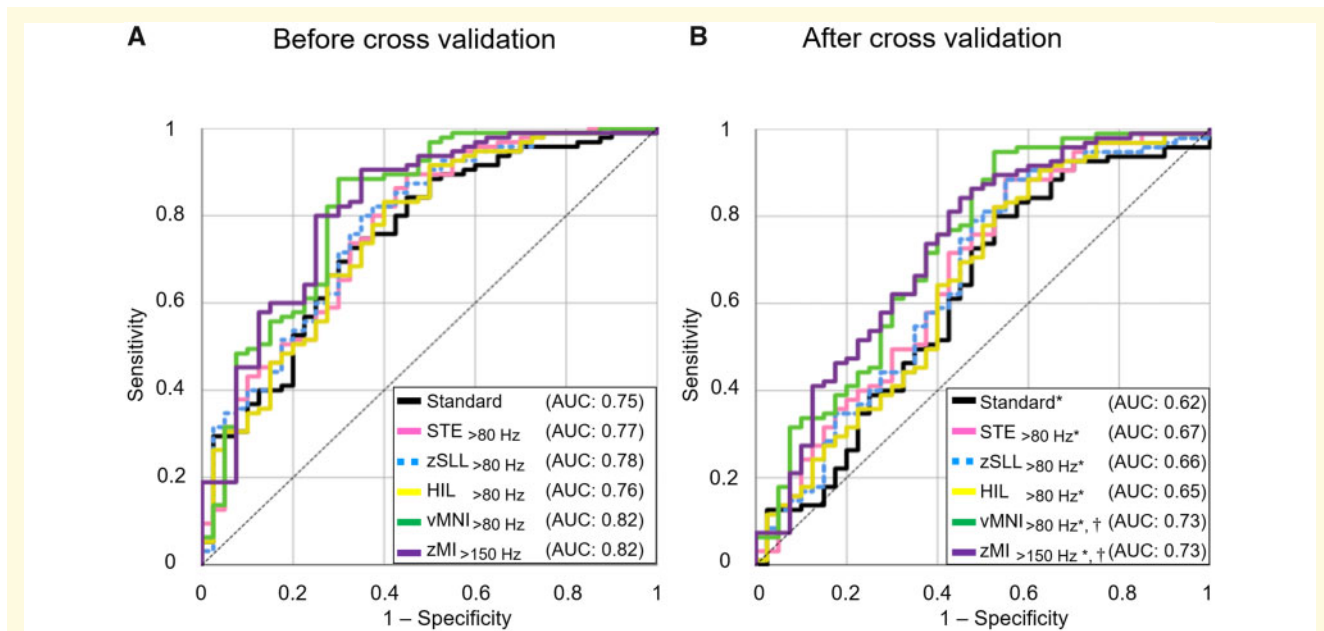


**Figure 4** The accuracy of models incorporating interictal electrophysiology biomarkers. (A) A given ROCs curve delineates the accuracy of seizure outcome classification of a given model. Black line: Standard model. Pink line:  $\text{STE}_{>80\text{Hz}}$  model. Green line:  $\text{zSLL}_{>80\text{Hz}}$  model incorporating  $\text{SLL}_{>80\text{Hz}}$  (i.e. z-score normalized  $\text{SLL}_{>80\text{Hz}}$ ). Yellow line:  $\text{HIL}_{>80\text{Hz}}$  model. Orange line:  $\text{vMNI}_{>80\text{Hz}}$  model incorporating  $\text{vMNI}_{>80\text{Hz}}$  (i.e.  $\text{MNI}_{>80\text{Hz}}$  verified to have distinct high-frequency oscillatory components unattributable to the effect of high-pass filtering). Purple line:  $\text{zMI}_{>150\text{Hz}}$  model. The areas under the ROC curves were greater than 0.5 (Bonferroni-corrected  $P < 0.001$  on Mann-Whitney U test). Both HFO- and MI-based models improved the outcome classification by the standard model (accuracy: 0.75 → up to 0.82). (B) The ROC curves with a leave-one-out approach used. Both HFO- and MI-based models improved the outcome prediction based on the standard model (accuracy: 0.62 → up to 0.73). Comparison of 134 'sensitivity × specificity' values consisting of each ROC plot<sup>31</sup> determined whether the size of AUC for a given HFO/MI-based model differed from the chance level (i.e. 0.5) and that of the standard model. We found that all five HFO/MI-based models had AUC larger than 0.5 (\*, Bonferroni-corrected  $P < 0.001$  on t-test).  $\text{vMNI}_{>80\text{Hz}}$  and  $\text{zMI}_{>150\text{Hz}}$  models had AUC larger than that of the standard model (†, Bonferroni-corrected  $P < 0.001$  on t-test).



(mean rate across all non-epileptic sites: 5.1/5 min) and HIL (5.9/5 min) detectors detected HFO<sub>>80Hz</sub> more than the STE (0.9/5 min) and MNI (0.7/5 min) ( $P < 0.001$  on the linear mixed model analysis).

## Values of HFO, zHFO and vHFO

HFO<sub>>80Hz</sub> improved the outcome classification accuracy of the standard model better than HFO<sub>>150Hz</sub> and HFO<sub>>250Hz</sub>. Thus, we described the performance of HFO<sub>>80Hz</sub> in the Results Section below.

The classification accuracy of the STE<sub>>80Hz</sub>, SLL<sub>>80Hz</sub>, HIL<sub>>80Hz</sub> and MNI<sub>>80Hz</sub> models was 0.77, 0.75, 0.76 and 0.80 (Supplementary Fig. 3A–D). Higher Subtraction-STE<sub>>80Hz</sub>, Subtraction-HIL<sub>>80Hz</sub> and Subtraction-MNI<sub>>80Hz</sub> were independently associated with a greater chance of success (OR: 1.23 [95%CI: 1.03–1.46]; OR: 1.05 [1.01–1.10]; OR: 1.18 [1.04–1.33]) (Table 2).

The classification accuracy of the zSTE<sub>>80Hz</sub>, zSLL<sub>>80Hz</sub>, zHIL<sub>>80Hz</sub> and zMNI<sub>>80Hz</sub> models was 0.77, 0.78, 0.75 and 0.80 (Supplementary Fig. 4A–D). Higher Subtraction-zSLL<sub>>80Hz</sub> and Subtraction-zMNI<sub>>80Hz</sub> were associated with a greater chance of success (OR: 1.15 [95%CI: 1.03–1.29]; OR: 1.22 [1.07–1.38]) (Table 2 and Fig. 5).

The classification accuracy of the vSTE<sub>>80Hz</sub>, vSLL<sub>>80Hz</sub>, vHIL<sub>>80Hz</sub> and vMNI<sub>>80Hz</sub> models was 0.77, 0.77, 0.75 and 0.82 (Supplementary Fig. 5). Higher Subtraction-vSTE<sub>>80Hz</sub>, Subtraction-vSLL<sub>>80Hz</sub> and Subtraction-vMNI<sub>>80Hz</sub> were associated with a greater chance of success (OR: 1.52 [95%CI: 1.05–2.20]; OR: 1.10 [1.01–1.19]; OR: 10.80 [1.16–1.01 × 10<sup>2</sup>]) (Table 2).

## Outcome classification using the MI and zMI models

MI<sub>>150Hz</sub> improved the standard model better than MI<sub>>80Hz</sub> and MI<sub>>250Hz</sub>. Thus, we described the performance of MI<sub>>150Hz</sub> in the Results section below. The MI<sub>>150Hz</sub> and zMI<sub>>150Hz</sub> models improved the standard model, and the outcome classification accuracy was 0.81 and 0.82 (Supplementary Figs. 3E and 4E). Higher Subtraction-MI<sub>>150Hz</sub> (OR:  $7.23 \times 10^{11}$  [95%CI:  $1.23 \times 10^2$ – $4.26 \times 10^{21}$ ]) and Subtraction-zMI<sub>>150Hz</sub> (OR: 1.28 [1.05–1.56]) were independently associated with a greater chance of success (Table 2 and Fig. 5).

## Cross-validation

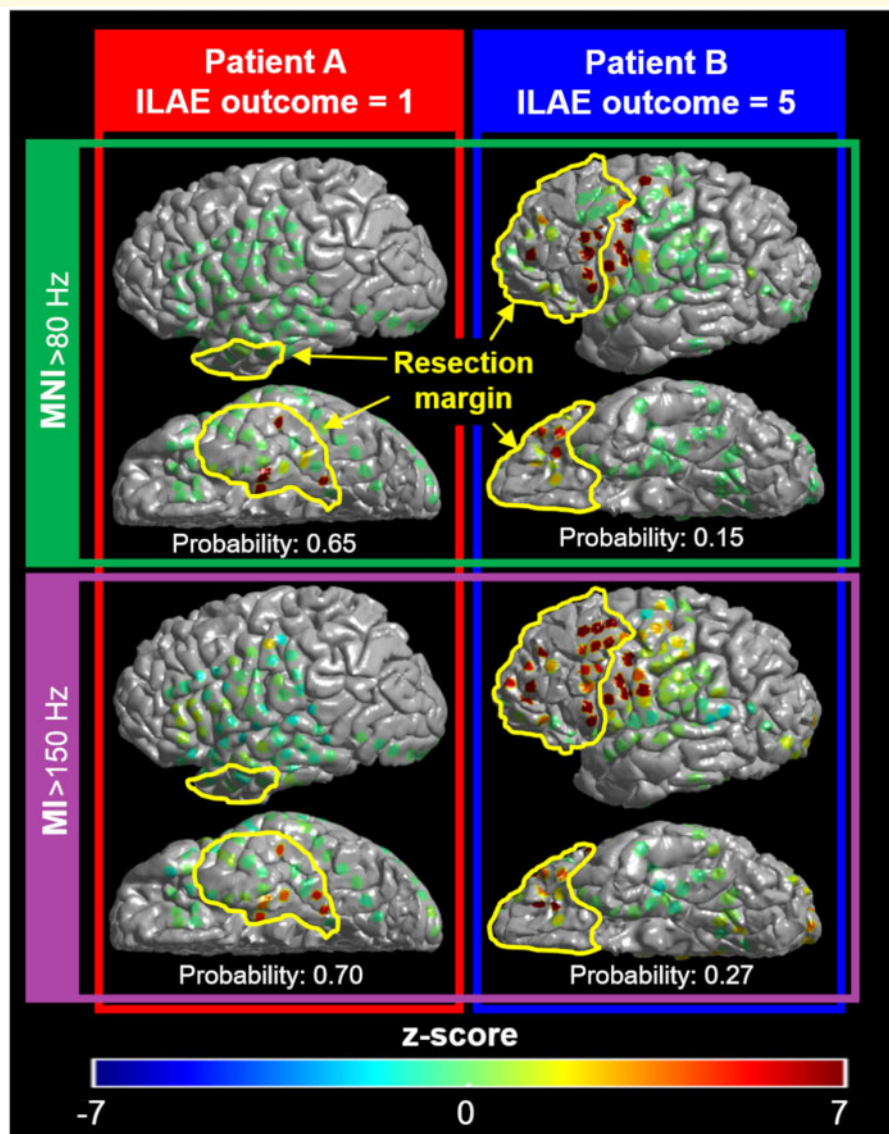
We cross-validated STE<sub>>80Hz</sub>, zSLL<sub>>80Hz</sub>, HIL<sub>>80Hz</sub>, vMNI<sub>>80Hz</sub> and zMI<sub>>150Hz</sub> models because a given analytic approach optimized the outcome classification performance. Following the leave-one-out cross-validation, the accuracy of outcome prediction of the standard, STE<sub>>80Hz</sub>, zSLL<sub>>80Hz</sub>, HIL<sub>>80Hz</sub>, vMNI<sub>>80Hz</sub> and zMI<sub>>150Hz</sub> model was 0.62, 0.67, 0.66, 0.65, 0.73 and 0.73, respectively (Bonferroni-corrected  $P < 0.001$  [significantly greater than 0.5]; Fig. 4B). Furthermore, the accuracies of outcome prediction of the vMNI<sub>>80Hz</sub> and zMI<sub>>150Hz</sub> models were higher than that of the standard model (Bonferroni-corrected  $P < 0.001$ ; Fig. 4B).

Figure 6 demonstrates a generous agreement between the model-based likelihood of success and the observed frequency of success on an individual basis. Supplementary Fig. 6 presents the relationship between

**Table 2 Accuracy of the HFO, zHFO, vHFO, MI and zMI models in outcome classification**

Model	HFO model			zHFO model			vHFO model		
	P	OR	95% CI	P	OR	95% CI	P	OR	95% CI
STE <sub>&gt;80Hz</sub>	<b>0.02</b>	1.23	1.03–1.46	0.08	1.27	—	<b>0.03</b>	1.52	1.05–2.20
STE <sub>&gt;150Hz</sub>	0.11	2.32	—	NA	NA	NA	0.23	2.75	—
STE <sub>&gt;250Hz</sub>	0.45	$4.71 \times 10^{-15}$	—	NA	NA	NA	>0.99	$8.58 \times 10^{-178}$	—
SLL <sub>&gt;80Hz</sub>	0.08	1.02	—	<b>0.01</b>	1.15	1.03–1.29	<b>0.03</b>	1.10	1.01–1.19
SLL <sub>&gt;150Hz</sub>	0.78	1.01	—	0.28	1.03	—	0.18	1.16	—
SLL <sub>&gt;250Hz</sub>	0.20	2.02	—	0.74	1.00	—	0.83	1.27	—
HIL <sub>&gt;80Hz</sub>	<b>0.02</b>	1.05	1.01–1.10	0.09	1.28	—	0.09	1.33	—
HIL <sub>&gt;150Hz</sub>	0.17	1.30	—	0.78	1.00	—	0.25	2.63	—
HIL <sub>&gt;250Hz</sub>	0.33	$5.39 \times 10^{-35}$	—	NA	NA	NA	>0.99	$3.00 \times 10^{-266}$	—
MNI <sub>&gt;80Hz</sub>	<b>0.008</b>	1.18	1.04–1.33	<b>0.002</b>	1.22	1.07–1.38	<b>0.04</b>	10.80	$1.16$ – $1.01 \times 10^2$
MNI <sub>&gt;150Hz</sub>	0.08	1.60	—	0.78	1.00	—	<b>0.005</b>	$1.82 \times 10^5$	$36.51$ – $9.07 \times 10^8$
MNI <sub>&gt;250Hz</sub>	0.38	1.58	—	0.76	1.00	—	0.42	$2.03 \times 10^2$	—
Model	MI model			zMI model					
	P	OR	95% C.I.	P	OR	95% C.I.			
MI <sub>&gt;80Hz</sub>	<b>0.01</b>	$4.75 \times 10^2$	$4.01$ – $5.64 \times 10^4$	<b>0.01</b>	1.20	1.04–1.39			
MI <sub>&gt;150Hz</sub>	<b>0.02</b>	$7.23 \times 10^{11}$	$1.23 \times 10^2$ – $4.26 \times 10^{21}$	<b>0.01</b>	1.28	1.05–1.56			
MI <sub>&gt;250Hz</sub>	<b>0.02</b>	$4.76 \times 10^{41}$	$1.25 \times 10^6$ – $1.81 \times 10^{77}$	<b>0.02</b>	1.23	1.03–1.46			

All toolboxes could generate a model that accurately classified the post-operative seizure outcome with significance ( $P$ -value  $< 0.05$ ). CI = confidence interval; HFO = high-frequency oscillation; MI = modulation index; OR = odds ratio;  $P$  =  $P$ -value. zHFO/zMI model: That incorporating z-score normalized HFO/MI instead of absolute HFO/MI. vHFO model: That incorporating HFO verified to have high-frequency oscillatory components unattributable to a high-pass filtering effect. NA (not available): we were unable to perform the z-score normalization for STE<sub>>150Hz</sub>, STE<sub>>250Hz</sub> and HIL<sub>>250Hz</sub> due to the lack of detected events in non-epileptic regions.  $P < 0.05$  indicates significance in bold typeface.



**Figure 5 Relationship between interictal electrophysiology biomarker, resection margin and post-operative seizure outcome.** The colour of each electrode site reflects the severity of interictal abnormality rated by the HFO rate as well as the MI. The yellow lines denote the resection margin in a given patient. Both  $MNI_{>80\text{ Hz}}$  and  $zMNI_{>80\text{ Hz}}$  models, incorporating interictal HFO rates defined by the MNI detector,<sup>12</sup> suggested that only patient A had a high probability to achieve surgical success. The  $MI_{>150\text{ Hz}}$  and  $zMI_{>150\text{ Hz}}$  models, incorporating the phase-amplitude coupling rated by MI,<sup>20</sup> made a similar outcome prediction. Indeed, Patient A achieved the ILAE class I outcome,<sup>36</sup> whereas Patient B had a ILAE class 5 outcome.

the model-based outcome prediction and the observed ILAE outcome scale. The Spearman rank test indicated that increased model-based probability of success was associated with better post-operative seizure outcome (Bonferroni-corrected  $P < 0.05$ ; Supplementary Fig. 6).

### Computational time

The computational time was 3.7s/channel for the STE-based HFO detection (95% CI: 3.55–3.85), 4.0 for the SLL (3.83–4.17), 4.2 for the HIL (4.04–4.36) and 89.3

for the MNI (84.73–93.87) and 1.2 for the MI quantification (1.15–1.25).

## Discussion

### Summary

Our overall results support the hypothesis that interictal HFO/MI measures improve the accuracy of the outcome classification based on the measurements available for standard care, including clinical, neuroimaging and ictal

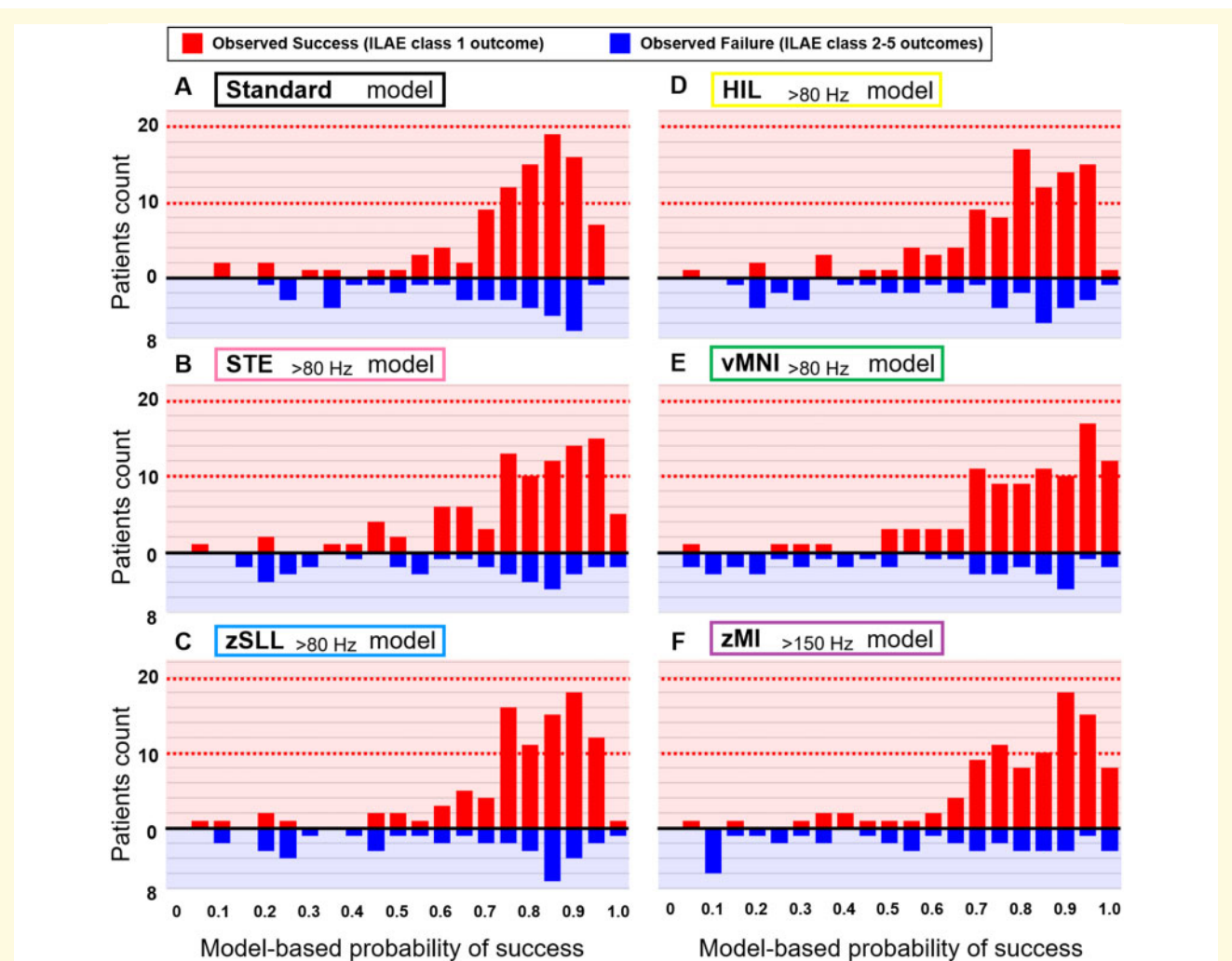


**Figure 6 Agreement between the model-based prediction and the observed frequency of surgical success.** X-axis: Model-based probability of surgical success for a given patient; each model was cross-validated by the leave-one-out procedure. Red bar: Number of patients achieving the ILAE class 1 outcome. Blue bar: The class 2 outcome or worse. **(A)** The standard model anticipated that 55 patients would achieve surgical success with a probability of greater than 0.8. Thereby, 42 out of these 55 patients (76%) indeed achieved surgical success. The standard model anticipated that 5 patients would achieve surgical success with a probability of smaller than 0.2. However, four out of these five patients (80%) still achieved surgical success. **(B)** The  $STE_{>80\text{ Hz}}$  model. **(C)** The  $zSLL_{>80\text{ Hz}}$  model. **(D)** The  $HIL_{>80\text{ Hz}}$  model. **(E)** The  $vMNI_{>80\text{ Hz}}$  model. **(F)** The  $zMI_{>150\text{ Hz}}$  model anticipated that 61 patients would achieve surgical success with a probability of greater than 0.8. Indeed, 51 out of these 61 patients (84%) achieved surgical success. The  $zMI_{>150\text{ Hz}}$  model anticipated that 10 patients would achieve surgical success with a probability of smaller than 0.2. Indeed, only two out of these 10 patients (20%) achieved surgical success.

iEEG information. The effect size of improvement in the outcome classification accuracy (from 0.75 up to 0.82) was comparable between HFO and MI. Our study supports the conceptual notion that the combined consideration of both interictal and ictal abnormalities would optimally localize the zone generating focal seizures.<sup>1</sup>

### Pros and cons of each of the tested biomarkers

We want to congratulate all investigators involved in the development of HFO detectors and MI quantification toolbox. None of the interictal electrophysiology

biomarkers was superior to others in all aspects, including precision, accuracy, speediness and interpretability.  $MI_{>150\text{ Hz}}$  and  $zMI_{>150\text{ Hz}}$  models improved the outcome classification accuracy from 0.75 to 0.81 and 0.82, respectively. MI, a continuous variable, might have characterized the spatial gradient in the severity of spike-and-wave discharges during a short interictal period better than the HFO rate, which is a discrete variable. 'MI of 1' may be more difficult to intuitively understand its meaning than '1 HFO event per minute'. We previously reported that iEEG epochs showing MI of 1 were characterized by abundant spike-and-wave discharges.<sup>31</sup> By definition, a higher magnitude of high-frequency

amplitude $_{\geq 80\text{Hz}}$  stereotypically coupled with slow-wave $_{3-4\text{Hz}}$  effectively increases the MI.<sup>19,20</sup> A recent iEEG study of 11 patients recently reported that the HFO amplitude classified the SOZ more accurately than the HFO rate.<sup>48</sup>

MNI $_{>80\text{Hz}}$ , zMNI $_{>80\text{Hz}}$  and vMNI $_{>80\text{Hz}}$  models had a classification accuracy of 0.80, 0.80 and 0.82. The rate of MNI $_{>80\text{Hz}}$  within the non-epileptic areas was smaller than those of SLL $_{>80\text{Hz}}$  and HIL $_{>80\text{Hz}}$ . Perhaps, the MNI detector is designed to be agnostic to continuous forms of HFO,<sup>12</sup> often taking place in the non-epileptic occipital areas.<sup>23</sup> Thus, some might perceive that MNI $_{>80\text{Hz}}$  would be easy to incorporate in clinical practice. The computational time of the MNI detector was longer than those of the other HFO or MI toolboxes. One may have to use a high-speed computer to complete the MNI-based HFO analysis to allow clinicians to make decisions in a real-time manner, particularly in the operation room.

SLL $_{>80\text{Hz}}$ , zSLL $_{>80\text{Hz}}$  and vSLL $_{>80\text{Hz}}$  had the outcome classification accuracy of 0.75, 0.78 and 0.77. The utility of SLL $_{>80\text{Hz}}$  became significant following the z-score normalization procedure, possibly because the default setting was designed to detect HFO events inclusively and broadly.<sup>13</sup>

STE $_{>80\text{Hz}}$ , zSTE $_{>80\text{Hz}}$  and vSTE $_{>80\text{Hz}}$  had the outcome classification accuracy of 0.77, 0.77 and 0.77. HIL $_{>80\text{Hz}}$ , zHIL $_{>80\text{Hz}}$  and vHIL $_{>80\text{Hz}}$  had the classification accuracy of 0.76, 0.75 and 0.75. Neither STE $_{>80\text{Hz}}$  nor HIL $_{>80\text{Hz}}$  benefitted from the z-score normalization or verification process. Both STE and HIL detectors required a short computational time; thus, they can promptly provide the results.

## Methodological considerations

We analysed the earliest 5-min slow-wave sleep epoch free from artefacts based on the visual assessment. This criterion is feasible for clinicians who would promptly need to decide the resection margin and adheres to the recommendation made in the guidelines of the use of HFO detectors.<sup>49</sup> Selection of a longer iEEG epoch for analysis (e.g. days)<sup>16</sup> could have optimized the normative HFO atlas and also detected more HFO events, particularly HFO $_{>250\text{Hz}}$  suggested to be a more specific but less sensitive biomarker than HFO $_{>80\text{Hz}}$ .<sup>7,8,50=52</sup> We are afraid that such an analysis of prolonged periods might increase the complexity of HFO/MI analysis. One should consider the effects of additional factors, including electromyographic artefacts such as those related to saccadic eye movements during REM sleep and wakefulness,<sup>53</sup> post-ictal states,<sup>54</sup> tissue swelling-related iEEG changes<sup>55</sup> and after-discharges associated with electrical stimulation mapping.<sup>56</sup> One must perform visual screening to identify and exclude artifactual channels during the tested interictal iEEG period to allow any of these toolboxes to quantify HFO or MI reliably. For the clinical translation of

HFO/MI analysis, a given team must complete the iEEG signal analysis before the resective surgery, which typically occurs within a few days after the intracranial electrode placement.

The effect of the applied sampling rate (1000 Hz) on HFO detection is expected to be modest.<sup>57</sup> Previous iEEG studies with a sampling rate of 2000 Hz indicated that the spectral frequency of neocortical HFO events mostly ranged below 300 Hz.<sup>50-52</sup> The vast majority of our patients were children, and only six had hippocampal sclerosis on MRI. iEEG recorded with a 1000-Hz sampling rate would require half of the data storage space needed for 2000-Hz.

What is the generalizability of our single-centre study? We computed the MI alone to assess the severity of phase-amplitude coupling between HFO and slow-wave, whereas other computation methods have been reported elsewhere.<sup>58-60</sup> With the default setting to detect HFO events, we generated the normative atlases, which demonstrated a noticeable variability in the spatial distribution of HFO rates across different toolboxes (Fig. 1). Some may raise the question of whether a specific toolbox should be recommended for iEEG clinical practice. Others may want to test different HFO detection settings further to optimize the outcome prediction method using our or their own dataset. We currently plan to determine our HFO/MI models' generalizability using iEEG data acquired at different institutions and also to assess their utility in children younger than 4 years of age. External validation would be necessary before making a strong recommendation for the standard practice.

The utility of HFO/MI on intraoperative iEEG or stereo-EEG recording remains uncertain. A study reported that the presence of intraoperative HFO $_{>250\text{Hz}}$  immediately after the resection was associated with a higher risk of failure; simultaneously, these investigators recommended that one should be aware of physiological HFO $_{>250\text{Hz}}$  generated by eloquent cortices.<sup>17</sup> Stereo-EEG allows us to sample the bottom of a sulcus which may include the epileptogenic zone, but its electrode density is low in a horizontal direction. We plan to develop the normative atlases of HFO/MI measured under the general anaesthesia and on stereo-EEG to determine the generalizability of the HFO/MI's utility.

## Conclusion

Interictal HFO and MI had a comparably additive utility in epilepsy presurgical evaluation. Our empirical data support the theoretical notion that the prediction of post-operative seizure outcomes can be optimized with the consideration of both interictal and ictal abnormalities.

## Supplementary material

Supplementary material is available at *Brain Communications* online.

## Acknowledgements

The authors are grateful to Deniz Altinok, MD, Jamie MacDougall RN, BSN, CPN and Karin Halsey, BS, REEGT at Children's Hospital of Michigan, Detroit Medical Centre, Wayne State University, for the collaboration and assistance in performing the studies described above.

## Funding

This research is supported by the National Institutes of Health Grants NS047550 (Asano), NS064033 (Asano) and NS089659 (Jeong).

## Competing interests

The authors have no conflicts of interest to report. We confirm that we have read the Journal's position on issues involved in ethical publication and affirm that this report is consistent with those guidelines.

## References

- Engel J Jr. Surgery for seizures. *N Engl J Med*. 1996;334(10):647–652.
- Jayakar P, Jayakar A, Libenson M, et al. International League Against Epilepsy. Epilepsy surgery near or in eloquent cortex in children-Practice patterns and recommendations for minimizing and reporting deficits. *Epilepsia*. 2018;59(8):1484–1491.
- Bernasconi A, Cendes F, Theodore W, et al. Recommendations for the use of structural magnetic resonance imaging in the care of patients with epilepsy: A consensus report from the International League Against Epilepsy neuroimaging task force. *Epilepsia*. 2019;60(6):1054–1068.
- Hufnagel A, Dümpelmann M, Zentner J, Schijns O, Elger CE. Clinical relevance of quantified intracranial interictal spike activity in presurgical evaluation of epilepsy. *Epilepsia*. 2000;41(4):467–478.
- Asano E, Benedek K, Shah A, et al. Is intraoperative electrocorticography reliable in children with intractable neocortical epilepsy? *Epilepsia*. 2004;45(9):1091–1099.
- Asano E, Juhász C, Shah A, Sood S, Chugani HT. Role of subdural electrocorticography in prediction of long-term seizure outcome in epilepsy surgery. *Brain*. 2009;132(Pt 4):1038–1047.
- Jacobs J, Staba R, Asano E, et al. High-frequency oscillations (HFOs) in clinical epilepsy. *Prog Neurobiol*. 2012;98(3):302–315.
- Zijlmans M, Worrell GA, Dümpelmann M, et al. How to record high-frequency oscillations in epilepsy: A practical guideline. *Epilepsia*. 2017;58(8):1305–1315.
- Staba RJ, Wilson CL, Bragin A, Fried I, Engel J Jr. Quantitative analysis of high-frequency oscillations (80–500 Hz) recorded in human epileptic hippocampus and entorhinal cortex. *J Neurophysiol*. 2002;88(4):1743–1752.
- Gardner AB, Worrell GA, Marsh E, Dlugos D, Litt B. Human and automated detection of high-frequency oscillations in clinical intracranial EEG recordings. *Clin Neurophysiol*. 2007;118(5):1134–1143.
- Crépon B, Navarro V, Hasboun D, et al. Mapping interictal oscillations greater than 200 Hz recorded with intracranial macroelectrodes in human epilepsy. *Brain*. 2010;133(Pt 1):33–45.
- Zelmann R, Mari F, Jacobs J, Zijlmans M, Chander R, Gotman J. Automatic detector of high frequency oscillations for human recordings with macroelectrodes. *Conf Proc IEEE Eng Med Biol Soc*. 2010;2010:2329–2333.
- Navarrete M, Alvarado-Rojas C, Le Van Quyen M, Valderrama M. RIPPLELAB: A comprehensive application for the detection, analysis and classification of high frequency oscillations in electroencephalographic signals. *PLoS One*. 2016;11(6):e0158276.
- Höller Y, Kutil R, Klaffenböck L, et al. High-frequency oscillations in epilepsy and surgical outcome. A meta-analysis. *Front Hum Neurosci*. 2015;9:574.
- Gloss D, Nevitt SJ, Staba R. The role of high-frequency oscillations in epilepsy surgery planning. *Cochrane Database Syst Rev*. 2017;10:CD010235.
- Gliske SV, Irwin ZT, Chestek C, et al. Variability in the location of high frequency oscillations during prolonged intracranial EEG recordings. *Nat Commun*. 2018;9(1):2155.
- van't Klooster MA, van Klink NEC, Zweiphenning WJEM, et al. Tailoring epilepsy surgery with fast ripples in the intraoperative electrocorticogram. *Ann Neurol*. 2017;81(5):664–676.
- Jacobs J, Wu JY, Perucca P, et al. Removing high-frequency oscillations: A prospective multicenter study on seizure outcome. *Neurology*. 2018;91(11):e1040–e1052.
- Canolty RT, Edwards E, Dalal SS, et al. High gamma power is phase-locked to theta oscillations in human neocortex. *Science*. 2006;313(5793):1626–1628.
- Miyakoshi M, Delorme A, Mullen T, Kojima K, Makeig S, Asano E. Automated detection of cross-frequency coupling in the electrocorticogram for clinical inspection. *Conf Proc IEEE Eng Med Biol Soc*. 2013;2013:3282–3285.
- Jacobs J, Kobayashi K, Gotman J. High-frequency changes during interictal spikes detected by time-frequency analysis. *Clin Neurophysiol*. 2011;122(1):32–42.
- Kural MA, Duez L, Sejer Hansen V, et al. Criteria for defining interictal epileptiform discharges in EEG: A clinical validation study. *Neurology*. 2020;94(20):e2139–e2147.
- Nonoda Y, Miyakoshi M, Ojeda A, et al. Interictal high-frequency oscillations generated by seizure onset and eloquent areas may be differentially coupled with different slow waves. *Clin Neurophysiol*. 2016;127(6):2489–2499.
- Iimura Y, Jones K, Takada L, et al. Strong coupling between slow oscillations and wide fast ripples in children with epileptic spasms: Investigation of modulation index and occurrence rate. *Epilepsia*. 2018;59(3):544–554.
- Frauscher B, von Ellenrieder N, Zelmann R, et al. High-frequency oscillations in the normal human brain. *Ann Neurol*. 2018;84(3):374–385.
- Guragain H, Cimbalnik J, Stead M, et al. Spatial variation in high-frequency oscillation rates and amplitudes in intracranial EEG. *Neurology*. 2018;90(8):e639–e646.
- Motoi H, Jeong JW, Juhász C, et al. Quantitative analysis of intracranial electrocorticography signals using the concept of statistical parametric mapping. *Sci Rep*. 2019;9(1):17385.
- Bénar CG, Chauvière L, Bartolomei F, Wendling F. Pitfalls of high-pass filtering for detecting epileptic oscillations: A technical note on “false” ripples. *Clin Neurophysiol*. 2010;121(3):301–310.
- Burnos S, Frauscher B, Zelmann R, Haegelen C, Sarnthein J, Gotman J. The morphology of high frequency oscillations (HFO) does not improve delineating the epileptogenic zone. *Clin Neurophysiol*. 2016;127(4):2140–2148.

30. Roehri N, Pizzo F, Lagarde S, et al. High-frequency oscillations are not better biomarkers of epileptogenic tissues than spikes. *Ann Neurol.* 2018;83(1):84–97.
31. Motoi H, Miyakoshi M, Abel TJ, et al. Phase-amplitude coupling between interictal high-frequency activity and slow waves in epilepsy surgery. *Epilepsia.* 2018;59(10):1954–1965.
32. Asano E, Chugani DC, Juhász C, Muzik O, Chugani HT. Surgical treatment of West syndrome. *Brain Dev.* 2001;23(7):668–676.
33. Sood S, Marupudi NI, Asano E, Haridas A, Ham SD. Endoscopic corpus callosotomy and hemispherotomy. *J Neurosurg Pediatr.* 2015;16(6):681–686.
34. Sood S, Ilyas M, Marupudi NI, et al. Anatomical hemispherectomy revisited—outcome, blood loss, hydrocephalus, and absence of chronic hemosiderosis. *Childs Nerv Syst.* 2019;35(8):1341–1349.
35. Nakai Y, Jeong JW, Brown EC, et al. Three- and four-dimensional mapping of speech and language in patients with epilepsy. *Brain.* 2017;140(5):1351–1370.
36. Wieser HG, Blume WT, Fish D, et al. Commission on Neurosurgery of the International League Against Epilepsy (ILAE). ILAE Commission Report. Proposal for a new classification of outcome with respect to epileptic seizures following epilepsy surgery. *Epilepsia.* 2001;42(2):282–286.
37. Ghosh SS, Kakunoori S, Augustinack J, et al. Evaluating the validity of volume-based and surface-based brain image registration for developmental cognitive neuroscience studies in children 4 to 11 years of age. *Neuroimage.* 2010;53(1):85–93.
38. Ikegaya N, Motoi H, Iijima K, et al. Spatiotemporal dynamics of auditory and picture naming-related high-gamma modulations: A study of Japanese-speaking patients. *Clin Neurophysiol.* 2019;130(8):1446–1454.
39. Jayakar P, Gotman J, Harvey AS, et al. Diagnostic utility of invasive EEG for epilepsy surgery: Indications, modalities, and techniques. *Epilepsia.* 2016;57(11):1735–1747.
40. Remick M, Ibrahim GM, Mansouri A, Abel TJ. Patient phenotypes and clinical outcomes in invasive monitoring for epilepsy: An individual patient data meta-analysis. *Epilepsy Behav.* 2020;102:106652.
41. Steinbart D, Steinbrenner M, Oltmanns F, Holtkamp M. Prediction of seizure freedom after epilepsy surgery—critical reappraisal of significance of intracranial EEG parameters. *Clin Neurophysiol.* 2020;131(11):2682–2690.
42. Swift JR, Coon WG, Guger C, et al. Passive functional mapping of receptive language areas using electrocorticographic signals. *Clin Neurophysiol.* 2018;129(12):2517–2524.
43. Nariai H, Nagasawa T, Juhász C, Sood S, Chugani HT, Asano E. Statistical mapping of ictal high-frequency oscillations in epileptic spasms. *Epilepsia.* 2011;52(1):63–74.
44. Kambara T, Sood S, Alqatan Z, et al. Presurgical language mapping using event-related high-gamma activity: The Detroit procedure. *Clin Neurophysiol.* 2018;129(1):145–154.
45. Stolk A, Griffin S, Van der Meij R, et al. Integrated analysis of anatomical and electrophysiological human intracranial data. *Nat Protoc.* 2018;13(7):1699–1723.
46. Kwan P, Brodie MJ. Neuropsychological effects of epilepsy and antiepileptic drugs. *Lancet.* 2001;357(9251):216–222.
47. Englot DJ, Breshears JD, Sun PP, Chang EF, Auguste KI. Seizure outcomes after resective surgery for extra-temporal lobe epilepsy in pediatric patients. *J Neurosurg Pediatr.* 2013;12(2):126–133.
48. Charupanit K, Sen-Gupta I, Lin JJ, Lopour BA. Amplitude of high frequency oscillations as a biomarker of the seizure onset zone. *Clin Neurophysiol.* 2020;131(11):2542–2550.
49. Remakanthakurup Sindhu K, Staba R, Lopour BA. Trends in the use of automated algorithms for the detection of high-frequency oscillations associated with human epilepsy. *Epilepsia.* 2020;61(8):1553–1569.
50. Worrell GA, Gardner AB, Stead SM, et al. High-frequency oscillations in human temporal lobe: Simultaneous microwire and clinical macroelectrode recordings. *Brain.* 2008;131(4):928–937.
51. Wu JY, Sankar R, Lerner JT, Matsumoto JH, Vinters HV, Mathern GW. Removing interictal fast ripples on electrocorticography linked with seizure freedom in children. *Neurology.* 2010;75(19):1686–1694.
52. Wang S, Wang IZ, Bulacio JC, et al. Ripple classification helps to localize the seizure-onset zone in neocortical epilepsy. *Epilepsia.* 2013;54(2):370–376.
53. Uematsu M, Matsuzaki N, Brown EC, Kojima K, Asano E. Human occipital cortices differentially exert saccadic suppression: Intracranial recording in children. *Neuroimage.* 2013;83:224–236.
54. Gotman J, Koffler DJ. Interictal spiking increases after seizures but does not after decrease in medication. *Electroencephalogr Clin Neurophysiol.* 1989;72(1):7–15.
55. Kovac S, Rodionov R, Chinnasami S, et al. Clinical significance of non-habitual seizures during intracranial EEG monitoring. *Epilepsia.* 2014;55(1):e1–e5.
56. Aungaroon G, Zea Vera A, Horn PS, et al. After-discharges and seizures during pediatric extra-operative electrical cortical stimulation functional brain mapping: Incidence, thresholds, and determinants. *Clin Neurophysiol.* 2017;128(10):2078–2086.
57. Nunez PL, Srinivasan R. *Electric fields of the brain: The neurophysics of EEG.* New York: Oxford University Press; 2006.
58. Amiri M, Frauscher B, Gotman J. Interictal coupling of HFOs and slow oscillations predicts the seizure-onset pattern in mesiotemporal lobe epilepsy. *Epilepsia.* 2019;60(6):1160–1170.
59. Watrous AJ, Deuker L, Fell J, Axmacher N. Phase-amplitude coupling supports phase coding in human ECoG. *Elife.* 2015;4:e07886.
60. Weiss SA, Orosz I, Salamon N, et al. Ripples on spikes show increased phase-amplitude coupling in mesial temporal lobe epilepsy seizure-onset zones. *Epilepsia.* 2016;57(11):1916–1930.